

## Journal Pre-proof

In-situ formation of nanoparticles from drug-loaded 3D polymeric matrices



Felipe Q. Pires , Idejan P. Gross , Livia L. Sa-Barreto ,  
Tais Gratieri , Guilherme M. Gelfuso , Sonia N. Bao ,  
Marcilio Cunha-Filho

PII: S0928-0987(23)00147-1  
DOI: <https://doi.org/10.1016/j.ejps.2023.106517>  
Reference: PHASCI 106517

To appear in: *European Journal of Pharmaceutical Sciences*

Received date: 18 April 2023  
Revised date: 29 June 2023  
Accepted date: 2 July 2023

Please cite this article as: Felipe Q. Pires , Idejan P. Gross , Livia L. Sa-Barreto , Tais Gratieri , Guilherme M. Gelfuso , Sonia N. Bao , Marcilio Cunha-Filho , In-situ formation of nanoparticles from drug-loaded 3D polymeric matrices, *European Journal of Pharmaceutical Sciences* (2023), doi: <https://doi.org/10.1016/j.ejps.2023.106517>

This is a PDF file of an article that has undergone enhancements after acceptance, such as the addition of a cover page and metadata, and formatting for readability, but it is not yet the definitive version of record. This version will undergo additional copyediting, typesetting and review before it is published in its final form, but we are providing this version to give early visibility of the article. Please note that, during the production process, errors may be discovered which could affect the content, and all legal disclaimers that apply to the journal pertain.

© 2023 Published by Elsevier B.V.  
This is an open access article under the CC BY-NC-ND license  
(<http://creativecommons.org/licenses/by-nc-nd/4.0/>)

## Highlights

- 3D printed tablets spontaneously generate drug-loaded nanoparticles in aqueous medium
- In-situ nanoparticles formation is caused by drug-plasticizer-polymer interactions
- Stable spherical-shaped nanoparticles were produced with high drug encapsulation
- Solubility and formulation treatment are relevant for nanoparticle formation
- In-situ formation of nanoparticles should be monitored in 3D polymeric systems

*Original article*

### ***In-situ* formation of nanoparticles from drug-loaded 3D polymeric matrices**

Felipe Q. Pires<sup>a</sup>, Idejan P. Gross<sup>a</sup>, Livia L. Sa-Barreto<sup>b</sup>, Tais Gratieri<sup>a</sup>, Guilherme M. Gelfuso<sup>a</sup>, Sonia N. Bao<sup>c</sup>, Marcilio Cunha-Filho<sup>a,\*</sup>

<sup>a</sup>University of Brasilia, School of Health Sciences, Laboratory of Food, Drugs, and Cosmetics (LTMAC). 70.910-900, Brasília, DF, Brazil.

<sup>b</sup>University of Brasilia, Faculty of Ceilandia. 72220-900, Brasília, DF, Brazil.

<sup>c</sup>University of Brasilia, Institute of Biological Sciences, Laboratório de Microscopia e Microanálise. 70910-900, Brasília, DF, Brazil.

\*Corresponding author. Tel.: +55 61 31071929. Email address: marciliofarm@hotmail.com (M. Cunha-Filho).

#### **ABSTRACT**

The in-situ formation of nanoparticles from polymer-based solid medicines, although previously described, has been overlooked despite its potential to interfere with oral drug bioavailability. Such polymeric pharmaceuticals are becoming increasingly common on the market and can become even more popular due to the dizzying advance of 3D printing medicines. Hence, this work aimed to study this phenomenon during the dissolution of 3D printed tablets produced with three different polymers, hydroxypropylmethylcellulose acetate succinate (HPMCAS), polyvinyl alcohol (PVA), and Eudragit RL PO® (EUD RL) combined with plasticizers and the model drug naringenin (NAR). The components' interaction, dissolution behavior, and characteristics of the formed particles were investigated employing thermal, spectroscopic, mechanical, and chromatographic assays. All the systems generated

stable spherical-shaped particles throughout 24 h, encapsulating over 25% of NAR. Results suggest encapsulation efficiencies variations may depend on interactions between polymer-drug, drug-plasticizer, and polymer-plasticizer, which formed stable nanoparticles even in the drug absence, as observed with the HPMCAS and EUD RL formulations. Additionally, components solubility in the medium and previous formulation treatments are also a decisive factor for nanoparticle formation. In particular, the treatment provided by hot-melt extrusion and FDM 3D printing affected the dissolution efficiency enhancing the interaction between the components, reverberating on particle size and particle formation kinetics mainly for HPMCAS and EUD RL. In conclusion, the 3D printing process influences the in-situ formation of nanoparticles, which can directly affect oral drug bioavailability and needs to be monitored.

**Keywords:** Naringenin; Drug Release; Fused Deposition Modeling; Oral bioavailability; Printlets.

## 1. Introduction

In the past decades, the use of polymeric materials as drug matrices has become common with the incorporation of new technologies for modified drug release. In fact, several market drug products are produced from polymeric substrates forming solid dispersions, adding therapeutic benefits such as modulation of drug release, increased solubility, and stability (Alshehri et al., 2020). Moreover, the use of different polymers in medicines has been escalated with the consolidation of hot-melt extrusion (HME) technology in pharmaceutical factories, allowing solid dispersions to be produced in a simplified, continuous, and solvent-free process (Tran et al., 2021).

Recent studies show that polymers' disaggregation in water could lead to micro and nanoparticle formation. In fact, supramolecular assemblies from HME solid dispersions spontaneously formed in an aqueous medium ranging from nanometer to micrometer were described (Kanzer et al., 2010; Tho et al., 2010; Frank et al., 2012a). Moreover, the presence of nanoplastics derived from physical or biological decomposition processes of polymeric materials thrown into the environment has been a source of a new type of pollution found in human tissues, constituting, in this case, an invisible threat to people's health (Gigault et al., 2021). Indeed, nanosized particles are known for being highly interactive structures that can easily disperse in different environments, being capable of entrapping material in their surfaces or cores, and permeating through biological membranes (Mitchell et al., 2021).

In the pharmaceutical field, the *in-situ* formation of nanoparticles from polymeric-based materials may impact the pharmacokinetics of a drug product (Schittny et al., 2020). Notably, for an oral dosage form, the presence of a nanoparticle can mean a modification of the drug available for absorption in the gastrointestinal cells, consequently affecting the drug's bioavailability (Sironi et al., 2017; Stewart and Grass, 2020). In fact, previous studies have shown that the permeation of the drug ABT-102 in Caco-2 monolayer cells from amorphous systems obtained by HME was dramatically higher than its crystalline state, without this being related to the formation of micelles (Frank et al., 2012b; Frank et al., 2014). In most dissolution studies with polymer-based medicines, it is assumed that the drug found in the dissolution medium is solvated and free to be absorbed by the body (Pandi et al., 2020). However, the truth is that between polymer matrix disaggregation and drug solubilization, intermediate states of drugs' microencapsulation and nanoencapsulation can occur (Nunes et al., 2022).

Such spontaneous formation of nanoscale polymeric structures in medicines has gone overlooked. Nevertheless, this occurrence can no longer be ignored, considering the relevance of polymer-based medicines, especially 3D printed dosage forms (Karalia et al., 2021). This new way of making medicines uses almost exclusively polymeric substrates, allowing high versatility in drug release with a therapy personalization (Pires et al., 2020). In particular, the most promising printing technique of fused deposition modeling (FDM) uses polymeric filaments obtained from HME as pharmaceutical ink (Araújo et al., 2019).

To illustrate the magnitude of this issue, 30 papers have been found in the “Web of Science database” in the last five years, focusing on dissolution studies of polymeric-base dosage forms produced with 3D printing and HME (Table S1). None of them verified the possible encapsulation of the drug in micro or nanoparticles in the dissolution tests, assuming the drug was free in the aqueous medium. Such negligence regarding the real physical state of the drug in a simulated gastrointestinal medium may lead to the unpredicted therapeutic performance of these medicines.

Particularly for the 3D printing process of oral dosage forms, such as in tablet forms - named printlets, a high percentage of the polymeric matrix is used in the composition, with variations in the drug amount (Karalia et al., 2021). Based on this, the odds of particle formation are high, and it is possible that the modifications brought by the printing process and the structure of the dosage form can also change the particle formation behavior.

In this scenario, there is an obvious need to study the mechanisms involved in the *in-situ* nanoparticle formation and the influence of the HME plus 3D printing processes on this phenomenon. Therefore, this work aimed to investigate the *in-situ* formation of nanoparticles during the dissolution of printlets for the first time. Three systems with different solubility characteristics and specific interactions between polymer, plasticizer, and drug were selected for this. Naringenin (NAR) was chosen as a model drug to be incorporated in the polymer matrices of hydroxypropylmethylcellulose acetate succinate (HPMCAS), polyvinyl alcohol (PVA), and Eudragit RL PO<sup>®</sup> (EUD RL), using glycerol and triethyl citrate as plasticizers.

## 2. Material and methods

### 2.1. Material

NAR [(2S)-5,7-Dihydroxy-2-(4-hydroxyphenyl)-2,3-dihydro-4H-chromen-4-one, purity  $\geq 98\%$ , lot MKCD1056] was obtained from Sigma-Aldrich (St. Louis, MO, USA). The polymer PVA (Parateck<sup>®</sup> MXP, lot F1952064) was donated by Merck (Darmstadt, Germany). HPMCAS (lot SF60G410004) and Eudragit RL PO<sup>®</sup> (EUD RL, Poly(ethyl acrylate-co-methyl methacrylate-co-trimethylammonioethyl methacrylate chloride), lot G170936626) were donated by Ashland Specialty Ingredients (Covington, LA, USA), and Evonik industries (Darmstadt, Germany), respectively. The plasticizers glycerin (GLY, lot 58591) and triethyl citrate (TEC, lot S7425151) were purchased from Dinâmica<sup>®</sup> (São Paulo, Brazil) and Merck (Darmstadt, Germany), respectively. All other chemicals and solvents were of analytical grade.

## 2.2. Preformulation studies

Three different polymers were selected for the filament formulation: HPMCAS, PVA, and EUD RL. Moreover, a plasticizer and the model drug NAR were also added to the formulation (Table 1). For each polymer, an appropriate plasticizer was selected according to its ability to increase the mobility of the polymer chains through the HME process, producing filaments more suitable for 3D FDM printing, i.e., TEC was used for the polymers HPMCAS and EUD RL, and GLY for PVA (Pereira et al., 2020).

Before the production, the interactions between the materials were assessed by determining the Hansen solubility parameter (HSP), and Fourier transform infrared spectroscopy (FTIR) analysis.

The HSP for NAR was estimated by Hoftyzer and Van Krevelen group-contribution method (van Krevelen and te Nijenhuis, 2009) (Table 2). For this purpose, the dispersion ( $\delta_d$ ), polar ( $\delta_p$ ), and hydrogen bond ( $\delta_h$ ) parameters were calculated by the equations:

$$\delta_d = \frac{\sum F_{di}}{V} \quad (1)$$

$$\delta_p = \frac{\sqrt{\sum F_{pi}^2}}{V} \quad (2)$$

$$\delta_h = \frac{\sqrt{\sum F_{hi}}}{V} \quad (3)$$

where  $F_{di}$ ,  $F_{pi}$ , and  $F_{hi}$  are, respectively, the dispersion, the polar, and the hydrogen bonding components of the molar attraction function for each contribution group “i”, and  $V$  is the molar volume of the respective molecule. Finally, the total Hansen

solubility parameter ( $\delta_t$ ) can be obtained from the vector sum of the three components previously calculated:

$$\delta_t = \sqrt{\delta_d^2 + \delta_p^2 + \delta_h^2} \quad (4)$$

The parameter values for HPMCAS and GLY were obtained from the studies of Klar and Urbanetz (Klar and Urbanetz, 2016). Those for PVA, EUD RL, and TEC were obtained from the studies of Kumar et al., Quinten et al., and Hansen, respectively (Hansen, 2007; Kumar et al., 2022; Quinten et al., 2021) (Table 2).

FTIR analyses were performed on Bruker model vertex 70 (Billerica, MA, USA), using the equipment ATR accessory, from 4,500 to 375  $\text{cm}^{-1}$  in a resolution of 2.0  $\text{cm}^{-1}$ . The FTIR spectrum of selected binary and ternary mixtures was obtained. The results were compared to the calculated average spectrum, calculated using the linear combination of the pure materials normalized absorption spectra, considering the proportion of each component in the formulation.

### 2.3. Filament production by HME

As described, the filament formulations comprised a combination of NAR, polymers, and suitable plasticizers (Table 1).

The mixtures were initially prepared using mortar and pestle. Then they extruded in a co-rotating conical twin-screw extruder with a die diameter of 1.8 mm (HAAKE MiniCTW, ThermoScientific, Waltham, MA, USA), without recirculation, coupled to a filament tractor system model FTR1 endowed with an automatic diameter gauge (Filmaq3D, Curitiba, Brazil). The screw rotation and processing temperature of HME, as well as the tractor system velocity, were chosen to guarantee the filament diameter's uniformity and the material's continuous flow. All filaments were stored in a desiccator with silica before the characterization.

### 2.4. Filament characterization

Filament diameters were measured every 10 cm using a digital caliper (Mitutoyo Sul Americana, São Paulo, Brazil). The mean diameter was calculated by the arithmetic mean of the measures. The visual characteristics were evaluated by optical microscopy using a stereoscope coupled to a video camera (Laborana/SZ – SZT, São Paulo, Brazil).

The filaments' printability was tested by measuring their mechanical resistance with the fracture force data ( $n = 5$ ) (Lima et al., 2022). The analysis was performed in a



universal testing machine (Shimadzu EZ test, Tokyo, Japan) equipped with a 5 kN load cell using wedge-type grips that move horizontally to tighten the grip on the filament (before analysis) and vertically to perform the elongation test. The cell moved at a constant crosshead speed of  $10.0 \text{ mm min}^{-1}$ . The filament size was 90 mm, the gap between the grips was 60 mm, and the initial force was 1.0 N.

### 2.5. *Printlets production by FDM 3D printing*

Cylinder shape printlets with a mean volume of  $0.569 \text{ cm}^3$  were designed using a free version of the software Tinkercad<sup>®</sup> (Autodesk<sup>®</sup> Inc, San Rafael, CA, USA) and were sliced using Slic3r<sup>®</sup> (Rome, Italy) software. The printlets were printed using the filaments prepared previously by HME at a Voolt FDM 3D printer model Gi3 (São Paulo, Brazil) with a brass nozzle with a diameter of 0.4 mm. The printing temperature was adapted to each polymer. The temperature of the printing bed was fixed at  $80 \text{ }^\circ\text{C}$ , and the printlets were printed three at a time. The layer height was set at 0.2 mm, and the infill pattern was rectilinear with a density of 50%. Three external layer shells were printed on all sides of the printlets, and the printing speed was set at  $15 \text{ mm s}^{-1}$  for printing moves and  $50 \text{ mm s}^{-1}$  for travel speed.

### 2.6. *Printlets characterization*

Printlets volumes were calculated by measuring the diameter and thickness of each printlet using a digital caliper (Mitutoyo Sul Americana, São Paulo, Brazil). The mean volume was obtained from 10 printlets for each formulation. The visual characteristics were evaluated by optical microscopy using a stereoscope coupled to a video camera (Laborana/SZ – SZT, São Paulo, Brazil).

The weight of each printlet was obtained using an analytical balance (Shimadzu, Tokyo, Japan). The individual weight and the mean weight obtained by the measure made in 10 tablets were used during the study. Drug content was determined in triplicate by dissolving the printlets in ethanol for the PVA samples and methanol for HPMCAS and EUD RL samples and determining the amount of NAR by HPLC as described in the 2.9 section.

### 2.7. *Dissolution studies and drug encapsulation*

Dissolution profiles of NAR as supplied, physical mixtures of the formulations, and the printlets were determined in a dissolution tester Ethik model 299 (Nova Ética, São Paulo, Brazil) using 900 mL of medium. For the HPMCAS samples, phosphate-

buffer solution 0.1 mol L<sup>-1</sup> (pH 6.8) was used as the dissolution medium (Thakkar et al., 2020), whereas, for the PVA and EUD RL samples, the medium was HCl 0.1 mol L<sup>-1</sup> (Pietrzak et al., 2015; Granados et al., 2022). The temperature was maintained at 37 °C, and apparatus 2 (paddle) was used, operating at 100 rpm. Samples containing approximately 25 mg of the drug were added to the dissolution vessels. Aliquots of 5.0 mL were withdrawn and immediately replaced by fresh dissolution medium at 1, 2, 3, 4, 5, 6, 8, 10, 12, and 24 h. The aliquots were filtered on a paper filter using a vacuum filtration system composed of a Büchner funnel, a borosilicate filtering flask, and a vacuum pump. After filtration, samples were diluted in an appropriate organic solvent to quantify the total amount of NAR by HPLC according to the method described in section 2.9.

To determine the nanoencapsulated drug fraction, the nanofiltration method was used with adaptation (Holzem et al., 2022). Another aliquot fraction was used to determine the amount of NAR possibly entrapped in the *in-situ* formed particles. For that, 2 mL of the sample was inserted on a Vivaspin 2 filter (MWCO 10,000, Sartorius Lab Instruments GmbH & Co, Goettingen, Germany) and centrifuged for 10 min at a rotation of 4,000 rpm in a Z306 centrifuge (Hermle Labortechnik GmbH, Wehinger, Germany). Next, the amount of NAR not entrapped (free NAR) was determined by the analyses of HPLC of the filtered material. Finally, the entrapped NAR was calculated according to Eq (5).

$$\text{Entrapped NAR (\% w/w)} = \frac{\text{Total amount of NAR} - \text{free NAR}}{\text{Total amount of NAR}} \times 100 \quad (5)$$

Experiments were performed in triplicate for each sample. Dissolution profiles were evaluated using their corresponding dissolution efficiency at 24 h (DE<sub>24</sub>) (Granados et al., 2022). Dissolution efficiency data were evaluated by GraphPad Prism 9 software (San Diego, CA, USA) using one-way ANOVA, followed by Turkey post-test. The statistical analysis of the drug encapsulation data was performed by two-way ANOVA followed by the Šídák post-test. The significance level (p) for both tests was fixed at 0.05, and data normality was previously demonstrated using the Shapiro-Wilk normality test.

### 2.8. Characterization of the *in-situ* formed particles

The particles generated from the polymeric systems were characterized in a release study under more concentrated conditions than the dissolution assay to allow the

assessment of the particle diameter, polydispersity index (PdI), zeta potential, and morphology. In this adapted dissolution experiment, NAR as supplied, physical mixtures of the formulations, and the printlets loaded or not with the drug were placed in a beaker containing 20 mL of the same mediums used in the dissolution studies described in the previous section. The systems were maintained in a water bath at  $37 \pm 3$  °C under constant magnetic stirring (100 rpm). Aliquots of 3 mL were withdrawn and immediately replaced by the fresh medium at 1, 4, 8, 12, and 24 h. Next, samples were analyzed using a Zetasizer Nano ZS (Malvern, UK). Hydrodynamic diameter determinations were performed using the dynamic light scattering (DLS) method to obtain the particle diameter, PdI, and average count rate, whereas the electrophoretic mobility method was used to determine the zeta potential. Statistics were evaluated using GraphPad Prism 9 software (San Diego, CA, USA) by two-way ANOVA, followed by Šidák post-test. The significance level ( $p$ ) was fixed at 0.05. Data normality was previously demonstrated using the Shapiro-Wilk normality test.

Additionally, the 12 h aliquot of the particle release experiments was used for morphological analysis. The samples were analyzed by transmission electron microscopy (TEM) using a JEM-1011 (JEOL, Tokyo, Japan). Before the analysis, diluted samples were deposited on Formvar-coated copper grids and received 3.0  $\mu$ L of uranyl acetate solution at 3% (w/v). After 3 min, the excess material was removed with filter paper, and the grids were air-dried. Then, the samples were taken to the equipment and analyzed at a magnitude of up to 3,000 times.

### 2.9. Drug determination

NAR was quantified by a reversed-phase chromatographic method with UV detection at 290 nm using the HPLC model LC-20AT (Shimadzu, Kyoto, Japan) (Quintao et al., 2022). The operating conditions of the method were as follows: 10  $\mu$ L of injection volume; reversed-phase  $C_{18}$  column (LC Column,  $300 \times 3.9$  mm, 10  $\mu$ m) kept at 40 °C; methanol/phosphoric acid 0.01 mol/L (65:35, v/v) as the mobile phase; and flow rate of 0.6 mL  $\text{min}^{-1}$ . The method was validated following the International Conference on Harmonization parameters and proved linear in the 0.5 to 30  $\mu\text{g mL}^{-1}$  range with a correlation coefficient ( $r$ ) = 0.999.

## 3. Results and discussion

### 3.1. Preformulation studies

Polymers with different characteristics used in marketed drug products that have already been assessed for 3D printing of medicines were selected for this study, i.e., HPMCAS (pH-dependent), PVA (water-soluble polymer), and EUD RL (insoluble polymer) (Pandi et al., 2020; Kuźmińska et al., 2021). Such polymers were combined with a suitable plasticizer to enable HME and FDM 3D printing (Pereira et al., 2020), totalizing six different formulations (Table 1). First, the interactions between the components of the formulations were assessed.

The molecular interactions between the components of a particle are known to have a decisive role in its final characteristics, such as shape, size, surface charge, and drug encapsulation (Hickey et al., 2015). Therefore, the HSP was obtained to predict those interactions. The results showed different possibilities for each polymer-based formulation (Fig. 1).

Minor variations of HSP ( $\Delta\delta_t$ ) were found between the polymer HPMCAS with the drug NAR ( $\Delta\delta_t = 4.73 \text{ MPa}^{1/2}$ ) and with the plasticizer TEC ( $\Delta\delta_t = 5.44 \text{ MPa}^{1/2}$ ). Values below  $7.0 \text{ MPa}^{1/2}$  suggest strong compound interaction, while values  $\Delta\delta_t > 10 \text{ MPa}^{1/2}$  are commonly associated with weak compound interaction (Greenhalgh et al., 1999). On the other hand, for the PVA polymer, the potential interaction with NAR was considered weak ( $\Delta\delta_t = 9.97 \text{ MPa}^{1/2}$ ); however, a strong interaction between the drug and the plasticizer glycerol was noted ( $\Delta\delta_t = 5.06 \text{ MPa}^{1/2}$ ). Finally, the HSP calculations suggested a strong interaction of EUD RL with its plasticizer TEC ( $\Delta\delta_t = 0.71 \text{ MPa}^{1/2}$ ); nevertheless, a low probability of interaction was observed between this polymer and the drug or between the drug and the plasticizer.

For a further interaction investigation, the binary mixtures with  $\Delta\delta_t < 7.0 \text{ MPa}^{1/2}$  were evaluated by FTIR and compared with the respective calculated average spectrum (Fig. 2).

In Fig. 2a, all the expected bands for NAR and HPMCAS were observed for the NAR + HPMCAS physical mixture, and no shifts were identified between the calculated and experimental spectra. This result was expected since the values of the component  $\delta_d$  suggest that the interactions between NAR and HPMCAS are mainly dispersive (Table 2), not being able to promote significant dipole changes to be detected by infrared spectroscopy.

On the other hand, as highlighted in Fig. 2b, a shoulder at  $3,596 \text{ cm}^{-1}$  appeared for the HPMCAS + TEC sample in the region of the O-H stretching. This finding may be associated with possible hydrogen bonds between the polymer and plasticizer,

corroborating the similar  $\delta_h$  values calculated for both components (Table 2). Similarly, a shoulder was also observed at  $3,267\text{ cm}^{-1}$  for EUD + TEC sample (Fig. 2d). The shoulder may be caused by the interaction between chemical groups of both molecules, most probably hydrogen bonds, since the -OH group of the plasticizer can act as a hydrogen bond donor that can interact with the many hydrogen bond acceptors presented in the polymer structure (Guerin et al., 2016).

As shown in Fig. 2c, the calculated average spectrum was almost the same as obtained for the NAR + GLY sample, suggesting a low interaction and/or solubility of the NAR in glycerol. However, for the ternary physical mixture PVA + NAR + GLY, the FTIR spectrum (Fig. 3) reveals small shifts in the C-O stretching and C-O-H bending bands, suggesting hydrogen bonds and/or other dipolar interactions.

The strong band at  $1,037\text{ cm}^{-1}$  was attributed to the glycerol C-O stretching shift observed at  $1,029\text{ cm}^{-1}$  for the pure GLY (Fig. S1). In addition, the C-O-H bending of the PVA appears at  $1,247\text{ cm}^{-1}$  for the physical mixture (Fig. 3b), which corresponds to a shift of  $8.0\text{ cm}^{-1}$  compared to the calculated average spectrum and the pure PVA (Fig. S1). The frequency of this mode can be shifted to higher energies by increasing the bond angle or by expanding the molecule's dipole moment, which, in turn, may be associated with specific hydrogen bond interactions between the components.

It is important to emphasize that the discreet quality of those shifts evidenced by the interactions does not compromise the stability of the components. Nevertheless, such interactions became more expressive with the HME and 3D printing processes.

The preformulation results evidence three different scenarios for the study, with different interactions governing the behavior of those formulations, especially on the formation and characteristics of the particles, including the mutual interaction of NAR-polymer and polymer-plasticizer influencing the HPMCAS samples and the NAR-plasticizer and polymer-plasticizer affecting the PVA and EUD RL samples, respectively.

### 3.2. The HME filaments

The filaments were obtained by HME by feeding the equipment with the material blend previously mixed. The constant feeding and the traction provided by filament tractor equipment allowed producing filaments with uniform diameters ( $SD < 0.11\text{ mm}$  for all filaments), which is one of the main factors that affect products' 3D printability (Bandari et al., 2021). The obtained filaments had a translucent and homogeneous aspect with a mean diameter between 1.70 and 1.46 mm (Table 3). This

result is close to the ideal range recommended for the printing process (1.80 to 1.60 mm), allowing the production of appropriate printlets (Ponsar et al., 2020).

Furthermore, the filaments also had an ideal mechanical property. All the samples underwent an elastic deformation during the fracture force analysis, supporting forces higher than 22 N (Table 3), far superior to the minimum required force value for 3D printing of 5 N (Y. Yang et al., 2021). This result reinforces the probable good printability of the produced filaments.

### 3.3. The printlets characterization

In agreement with what was expected, all the printlets obtained by the 3D printing process had a homogeneous appearance and uniformity in both weight and volume (Table 4). Furthermore, the weight and volume standard deviations were below 0.027 g and 0.009 cm<sup>3</sup>, respectively. Also, the drug content was within the pharmacopeial range for all the printlets, ensuring quality requirements for pharmaceutical dosage forms (Pires et al., 2020).

### 3.4. The dissolution assays

The nanoparticles formation over 24 h was studied by dissolution assay to simulate the oral drug release profile. Importantly, we analyzed the samples to distinguish the amount of NAR that was actually dissolved from that encapsulated in *in-situ* formed nanoparticles (Fig. 4). Noteworthy, the amount of drug encapsulated almost did not change with time and is represented in Fig. 4 by the mean values determined during the dissolution test.

In the case of the polymers HPMCAS and PVA, similar levels of drug encapsulation of around 25% were observed both in the physical mixture of the formulation components and in the formulation submitted to the production process of extrusion and 3D printing (printlets). This effect can be attributed to an *in-situ* interaction of NAR with such polymers and/or the respective plasticizers, as predicted by the HSP evaluation and confirmed by the FTIR analysis. Although NAR is more soluble in the release medium used for the HPMCAS systems (pH=6.8), the encapsulated drug content was very close to that observed in the PVA systems. This behavior can be explained by the higher polymer-drug and polymer-plasticizer interactions for the HPMCAS system, which could help maintain the cohesiveness of the nanostructure.

The drug dissolution improvement was more prominent in the physical mixture with PVA, probably due to the interactions between the NAR and the plasticizer GLY suggested by the HSP values. Furthermore, the effect may have been even more perceptible due to the slower dissolution profile of the drug in the acid medium. Indeed, for the physical mixtures containing EUD RL, such dissolution improvements did not occur due to the low interaction of the NAR with the other components of the formulation observed in the preformulation studies and the low solubility of this polymer in the medium (Berg et al., 2021).

In the EUD RL system, polymer and plasticizer have strong interactions with each other and are less soluble in the release medium. In fact, the polymer-polymer and polymer-plasticizer interactions, combined with the lower solubility of these components in the medium, favor cohesive forces, inhibiting the dissolution process and keeping NAR enclosed in EUD RL/TEC matrix. As a result, even though the NAR did not present strong interactions with the EUD/RL matrix, its release into the environment would depend on a diffusion process. In this context, unlike what was seen for the other polymers, the extrusion and 3D printing processes play an important role, favoring drug encapsulation. Indeed, while EUD RL physical mixtures lead to 24% of drug encapsulation, the printlets reached 42% (Fig. 4).

From these results, it is possible to suggest that the dissolution mechanism that leads to the *in-situ* formation of the nanoparticles observed in this study may depend on i) the nature of polymer-plasticizer, polymer-drug, drug-plasticizer interactions; ii) the solubility of the components in the release medium; and iii) the previous formulation treatment.

A drug-controlled release profile was observed for the printlets produced with HPMCAS and EUD RL, as expected (Fig. 4), due to the physical structure of the 3D printed dosage form. The printlets are formed by three layers of external shells and an infill of 50%, hindering a complete diffusion of the medium to the more porous inner part of the printlets. Depending on the solubility grade of the polymer on the medium, this structure can slow down the solubilization process, controlling the drug release (Thakkar et al., 2020). In fact, for the printlets produced using PVA, a highly soluble polymer, the control of NAR release was observed only in the first 2 h of the experiment, different from the other polymers that could control the drug release over 24 h.

The polymer disintegration, together with the printing settings, can significantly modify the dissolution profile of printlets, as observed in this study with NAR (Jamróz et al., 2020; Thakkar et al., 2020). However, the *in-situ* formation of drug-rich particles on a nanometric scale can play an important role in the bioavailability of such dosage forms. Studies show that depending on their characteristics, nanostructured drug particles can provide a more efficient drug release or a sustained one, directly affecting the pharmacokinetics (Sironi et al., 2017; Stewart and Grass, 2020).

One of the possible mechanisms related to the formation of those nanoparticles during the dissolution process is a burst release of the amorphous drug by diffusion from the polymeric matrix. At the interface of the polymeric system with the medium, there is a drug-saturated region, creating an environment conducive to drug encapsulation due to the interaction with the polymer/plasticizer. Hence, particles are spontaneously formed in the dissolution medium and stabilized. This theory would explain the formation process of nanoparticles observed in physical mixture samples (Pandi et al., 2020; Schittny et al., 2020) (Fig. 5). This process largely depends on the drug and the polymer characteristics, defining the profile and stability of the released particles (R. Yang et al., 2021).

Another plausible theory is the formation of the particles by an erosive process of the material. In this mechanism, the solvent enters the polymer matrix, swelling and causing the fragility of the solid structure (Fig. 5). The solvent action causes erosion on the material surfaces, and nanosized pieces of the material are released into the medium. Such particles retain their structure through the molecular interactions between the components, maintaining part of the drug entrapped inside the particles. Therefore, this process is highly dependent on the intensity of those molecular interactions (Göpferich, 1996).

Regardless of the formation pathway, the investigation of how the changes undergone by the 3D printing process can affect the formation and characteristics of those particles has, to our knowledge, not been described so far.

Considering all the polymers in this study, the lower mean percentage of NAR encapsulation was 22%, which is enough to impact any medical treatment. Indeed, such encapsulated drug will be released in a controlled way, directly affecting the drug uptake and bioavailability (Qian et al., 2021).

Since the particles' formation is related to the amount of drug, plasticizer, and polymer dispersed in the medium (Schittny et al., 2020), the constant amount of drug



encapsulated along the dissolution implied that the particles are formed following the same kinetics. Additionally, the stability provided by the specific molecular interactions between the components for each system kept the NAR encapsulated for 24 h, possibly directly affecting the drug uptake throughout the entire gastrointestinal tract transit.

### 3.5. The nanoparticles characterization

The apparent solubilization states of the drug, from molecularly dissolved passing by complexation, micellization, or nanostructured states, can lead to quite different bioavailability (Buckley et al., 2013). Therefore, to accurately assess particle populations at the nanoscale, adapted dissolution conditions were performed in order to generate colloidal dispersions concentrated enough to provide valid DLS results. To assess the physical characteristics of the spontaneously formed nanoparticles, a release test was performed with printlets and selected control samples, including the printlets without NAR and the physical mixtures containing or not NAR. First, it was verified whether the amount of nanoparticle formation was sufficient to perform the analysis. It occurs when the count rate shows values above 100 kcps, ensuring a precise measurement of the particle's characteristics (Zheng et al., 2016; Ullmann et al., 2019).

Based on that, NAR as supplied, physical mixtures without NAR, and printlets without NAR were excluded from the data analyses of all the polymers since the count rate values for these samples did not achieve the minimum required value. In such cases, the formation of nanostructures was found to be negligible. Exceptionally, printlets produced with HPMCAS and EUD RL (Fig. S2) could produce appreciable amounts of nanoparticles without NAR. In such cases, the stability of the *in-situ* nanostructures is explained by the polymer-plasticizer molecular interaction, as observed by the HSP and FTIR analyses. These findings contrast with PVA samples, in which the plasticizer-drug interaction is highly significant for nanoparticle formation, generating particles only for NAR-loaded formulations.

In contrast, the samples capable of generating *in-situ* nanoparticles reached high values of count rate, i.e., forming a considerable population of particles with a reasonable size uniformity (PDI values of around 0.6).

Considering the HPMCAS samples with NAR, a nanoparticle diameter coherence was observed between the hydrodynamic diameter and TEM determinations (Figs 6 and 7). The particles exhibited a spherical shape with well-defined borders (Fig. 7) and a particle size between 500 and 800 nm. The particle size generated from

physical mixtures was relatively stable over time, at around 600 nm (Fig. 6), while nanoparticles generated from printlets increased from 586 to 812 nm.

HPMCAS has shown a great tendency to interact with poorly soluble drugs such as NAR, as confirmed by HSP data. Accordingly, succinyl groups may form a strong drug-polymer interaction, especially for the M-grade HPMCAS used in this study. Additionally, the polymer-plasticizer interaction also has a significant role in the formulation. It seems to be sensitive to the HME and printing processes, explaining the difference in particle size between the physical mixture and printlet samples. The M-grade polymer is also rich in hydrophilic acetyl groups interacting intensely with the aqueous medium, justifying the increase in particle size observed on the particles during the experiment by a swollen effect, a consequence of this interaction (Nunes et al., 2022).

Still, regarding the cellulosic polymer systems with NAR, significant differentiation was also found among samples' zeta potential values. The mean values obtained throughout the experiment for the physical mixture and printlet were -21.7 mV and -10.6 mV, respectively. These findings suggest that the differences in the particles formed between the systems are not only related to the particle size but also their structural conformation. Considering that the HPMCAS has functional groups that, in an aqueous solution, it can appear negatively charged, the value difference between samples is probably related to the amount of polymer on the particle structure (R. Yang et al., 2021). As suggested by the irregular particle borders in TEM images, the physical mixture tends to have a high amount of polymeric material on the surface, which could enhance the particles' negative charge.

Regardless of the zeta potential difference between the particles, such nanostructures were stable in gastrointestinal simulation conditions (dissolution assay) for 24h. Furthermore, previous studies corroborate the stability of HPMCAS nanoparticles (Wilson et al., 2021).

For the HPMCAS printlets without NAR, a significative population of particles was detected by the DLS analyses only after 24 h of the dissolution process, evidencing a low-speed kinetics on the particle's formation, only achieving a significative number after a long dissolution process. The particles had a diameter of about 770 nm and a zeta potential of about -11.0 mV. Those particles are formed probably due to an erosion process of the polymeric material keeping its characteristics due to the drug-plasticizer interactions previously demonstrated by the preformulation analysis.

With PVA, an important difference was observed in the mean particle size of physical mixtures and printlets during the first hours of the assay (596 and 933 nm, respectively). However, a progressive reduction in the particles generated from the printlets occurred practically equaled their size to those produced from the physical mixtures (Fig. 6). It occurs probably due to the progressive solubilization of the polymer and the plasticizer in the medium, which may have become slower than expected due to the dissolution test adapted to more concentrated sample conditions in order to make DLS analyzes feasible. Accordingly, a marked structural difference was noticed in the morphological analyses (Fig. 7). Printlets produced nanoparticles with a more determined border, in contrast with the physical mixtures, which exhibited particles with a less uniform and diffuse surface.

Based on the zeta potential data, PVA's physical mixtures and printlets produced neutral surface particles (Fig. 6). During the dissolution assay, both samples exhibited zeta potential values  $>10$  mV, a common value found for other nanosized PVA samples since on acid medium the acetic groups of the molecule are neutralized, reducing the superficial charge of the nanoparticles (Madlova et al., 2009). Notwithstanding, as occurred to the other polymers samples, the particles were preserved during 24 h, probably due to the stabilization achieved thanks to the interaction between the drug, and the plasticizer GLY, as suggested by the HSP and FTIR analyses (Saboo et al., 2021).

Interestingly, the EUD RL samples suggested a different scenario regarding nanoparticle formation. Since this polymer is mostly insoluble in the medium, the solvent is not too efficient in destroying the polymeric matrix. As a result, formulations undergo a swelling process, but most of their structure is maintained throughout 24 h. However, the formation of the nanoparticles has been observed since the dissolution began and is very likely due to the already described erosion process (Fig. 5).

Based on the particle size of the samples made with NAR, a differentiation was founded during the particle's formation using EUD RL (Fig. 6). The physical mixture rapidly achieved the diameter sustained during most of the experiment (about 600 nm). In contrast, the printlets started with a lower particle size (about 320 nm), enhancing that value until the end of the experiment, achieving a high mean diameter value of 717 nm. The slower process of nanostructuring from the printlets can be attributed to a lower degree of polymer swelling after heat treatment by HME and 3D printing, which should favor the polymer-plasticizer interaction, as suggested by the preformulation

studies. Furthermore, the dissolution medium has less access to the compact structure of the printed object. Consequently, the erosion process is slower in such a sample affecting the particle formation process that could form a more stable particle only after a few hours of dissolution.

The morphological analyses of EUD RL nanostructures formed from the dissolution of the respective physical mixture showed evidence of a high amount of material on the particle's surface, in the same way as with the PVA particles. In contrast, the printlets had a more delimited particle.

Still, a zeta potential difference was found for the EUD RL samples with NAR. The physical mixture showed sustained high zeta potential throughout the experiment, with a mean of 30 mV. Such results indicate that those particles had good stability. The printlets, on the other hand, had an increasing behavior of the zeta potential during the experiment, staying most of the time on values <10 mV but achieving, after 24 h, a mean value >20 mV. These findings corroborate the hypotheses of slower formation and stabilization of the nanoparticles from printlets (Kamble et al., 2022). A combination of the molecular interactions and the low solubility is the most likely explanation for this behavior, i.e., the formation of the particles is delayed, producing a more uniform and stable surface after a few hours of dissolution.

Similarly, with the HPMCAS samples, the EUD RL printlets produced without NAR could form a significant amount of particles only after 24 h of the process (particle size of about 471 nm and Zeta potential of 7.0 mV), reinforcing that the polymer-plasticizer interaction intensified by the HME and 3D printing processing has a definitive role on the particle formation, probably also impacting the samples with NAR.

Based on the data collected in this study, it is possible to conclude that nanoparticle formation is highly dependent on the molecular interaction between the formulation components in association with the solubility of all the materials on the dissolution medium, probably defining the possible particle formation mechanism and kinetics.

From the point of view of the bioavailability of the drug product, one of the most important characteristics to be concerned with is the amount of encapsulated drug. Our results evidenced that the HME and 3D printing process importantly influence this parameter, especially for insoluble polymers, such as EUD RL. In such cases, the

particles are probably produced by a different mechanism, and the preparation process has a higher effect.

Despite the need to deepen and expand studies for other polymeric drug matrices, the results obtained here show sufficient consistency regarding the plausibility of the spontaneous generation of drug-loaded nanoparticles from these polymer-based pharmaceutical products. Thus, a study on drug encapsulation seems essential for every system that combines polymer, plasticizer, and drugs, considering that, in this study, all the samples, physical mixtures, or printlets, had some amount of the total drug entrapped on the formed particles during 24 h, directly affecting the amount of the drug free to be absorbed.

#### 4. Conclusion

To date, there are practically no studies deeply investigating the spontaneous formation of nanoparticles from polymeric matrices in the pharmaceutical field, although such occurrence has attracted attention in other segments. In contrast, using polymers in drug delivery systems is becoming increasingly common, especially with the recent explosion of 3D printed drug products. The study performed here evidences the interactions between the drug, plasticizer, and polymer, as well as with the medium, are capable of spontaneously forming nanoparticles during the dissolution of 3D dosage forms made with the polymers HPMCAS, PVA, and EUD RL, containing the poorly soluble NAR as the model drug. The formed particles had spherical shapes and sizes that varied according to the drug-polymer interaction. Especially the HME and printing processes greatly influenced those parameters, creating different sized particles and even affecting their zeta potential. In addition, the formed particles could encapsulate a considerable amount of NAR in all the samples, demonstrating that this phenomenon may directly affect oral drug bioavailability and therefore needs to be further monitored.

#### CRediT authorship contribution statement

**Felipe Q. Pires:** Investigation, Methodology, Writing – original draft. **Idejan P. Gross:** Investigation, Writing – review & editing. **Livia L. Sa-Barreto:** Resources, Project administration. **Tais Gratieri:** Conceptualization, Writing – review & editing. **Guilherme M. Gelfuso:** Conceptualization, Writing – review & editing. **Sonia N. Bao:** Methodology, Writing – review & editing. **Marcilio Cunha-Filho:** Conceptualization, Supervision, Writing – review & editing.

## Conflict of interest

The authors declare that they have no conflict of interest.

## Acknowledgements

The authors acknowledge the University of Brasília (Edital DPI/DPG), the Federal District Research Support Foundation (FAP-DF, Brazil, grants n. 00193-00000817/2021-64, and n. 00193-00000735/2021-10), the Financier of Studies and Projects (FINEP, grant n. 01.08.0457.00) and Coordination for the Improvement of Higher Education Personnel (CAPES, Brazil).

## References

- Alshehri, S., Imam, S.S., Hussain, A., Altamimi, M.A., Alruwaili, N.K., Alotaibi, F., Alanazi, A., Shakeel, F., 2020. Potential of solid dispersions to enhance solubility, bioavailability, and therapeutic efficacy of poorly water-soluble drugs: newer formulation techniques, current marketed scenario and patents. *Drug Deliv.* 27, 1625–1643. <https://doi.org/10.1080/10717544.2020.1846638>
- Araújo, M.R.P., Sa-Barreto, L.L., Gratieri, T., Gelfuso, G.M., Cunha-Filho, M., 2019. The digital pharmacies era: How 3D printing technology using fused deposition modeling can become a reality. *Pharmaceutics* 11. <https://doi.org/10.3390/pharmaceutics11030128>
- Bandari, S., Nyavanandi, D., Dumpa, N., Repka, M.A., 2021. Coupling hot melt extrusion and fused deposition modeling: Critical properties for successful performance. *Adv. Drug Deliv. Rev.* 172, 52–63. <https://doi.org/10.1016/j.addr.2021.02.006>
- Berg, S., Krause, J., Björkbom, A., Walter, K., Harun, S., Granfeldt, A., Janzén, D., Nunes, S.F., Antonsson, M., Van Zuydam, N., Skrtic, S., Hugerth, A., Weitschies, W., Davies, N., Abrahamsson, B., Bergström, C.A.S., 2021. In Vitro and In Vivo Evaluation of 3D Printed Capsules with Pressure Triggered Release Mechanism for Oral Peptide Delivery. *J. Pharm. Sci.* 110, 228–238. <https://doi.org/10.1016/j.xphs.2020.10.066>
- Buckley, S.T., Frank, K.J., Fricker, G., Brandl, M., 2013. Biopharmaceutical classification of poorly soluble drugs with respect to “enabling formulations”. *Eur. J. Pharm. Sci.* 50(1), 8-16. <https://doi.org/10.1016/j.ejps.2013.04.002>

- Frank, K.J., Westedt, U., Rosenblatt, K.M., Hölig, P., Rosenberg, J., Mägerlein, M., Fricker, G., Brandl, M., 2012a. The amorphous solid dispersion of the poorly soluble ABT-102 forms nano/microparticulate structures in aqueous medium: impact on solubility. *Int. J. Nanomedicine* 7, 5757-5768. <https://doi.org/10.2147/IJN.S36571>
- Frank, K.J., Rosenblatt, K.M., Westedt, U., Hölig, P., Rosenberg, J., Mägerlein, M., Fricker, G., Brandl, M., 2012b. Amorphous solid dispersion enhances permeation of poorly soluble ABT-102: true supersaturation vs. apparent solubility enhancement. *Int. J. Pharm.* 437(1-2), 288-293. <https://doi.org/10.1016/j.ijpharm.2012.08.014>
- Frank, K.J., Westedt, U., Rosenblatt, K.M., Hölig, P., Rosenberg, J., Mägerlein, M., Fricker, G., Brandl, M., 2014. What is the mechanism behind increased permeation rate of a poorly soluble drug from aqueous dispersions of an amorphous solid dispersion?. *J. Pharm. Sci.* 103(6), 1779-1786. <https://doi.org/10.1002/jps.23979>
- Gigault, J., El Hadri, H., Nguyen, B., Grassl, B., Rowenczyk, L., Tufenkji, N., Feng, S., Wiesner, M., 2021. Nanoplastics are neither microplastics nor engineered nanoparticles. *Nat. Nanotechnol.* 16, 501–507. <https://doi.org/10.1038/s41565-021-00886-4>
- Göpferich, A., 1996. Mechanisms of polymer degradation and erosion1. *Biomater. Silver Jubil. Compend.* 17, 117–128. <https://doi.org/10.1016/B978-008045154-1.50016-2>
- Granados, P.A., Pinho, L.A.G., Sa-Barreto, L.L., Gratieri, T., Gelfuso, G.M., Cunha-Filho, M., 2022. Application of hot-melt extrusion in the complexation of naringenin with cyclodextrin using hydrophilic polymers. *Adv. Powder Technol.* 33, 103380. <https://doi.org/10.1016/j.apt.2021.11.032>
- Greenhalgh, D.J., Williams, A.C., Timmins, P., York, P., 1999. Solubility parameters as predictors of miscibility in solid dispersions. *J. Pharm. Sci.* 88, 1182–1190. <https://doi.org/10.1021/js9900856>
- Guerin, A.C., Riley, K., Rupnik, K., Kuroda, D.G., 2016. Determining the Energetics of the Hydrogen Bond through FTIR: A Hands-On Physical Chemistry Lab Experiment. *J. Chem. Educ.* 93, 1124–1129. <https://doi.org/10.1021/acs.jchemed.5b01014>

- Hansen, C.M., 2007. Hansen solubility parameters: A user's handbook: Second edition, Second Edi. ed, Hansen Solubility Parameters: A Users Handbook, Second Edition. CRC Press. <https://doi.org/10.1201/9781420006834>
- Hickey, J.W., Santos, J.L., Williford, J.-M., Mao, H.-Q., 2015. Control of Polymeric Nanoparticle Size to Improve Therapeutic Delivery. *J. Control. Release* 219, 536–547. <https://doi.org/10.1016/j.jconrel.2015.10.006>.Control
- Holzem, F.L., Schaffland, J.P., Brandl, M., Bauer-Brandl, A., Stillhart, C., 2022. Microdialysis and nanofiltration allow to distinguish molecularly dissolved from colloid-associated drug concentrations during biomimetic dissolution testing of supersaturating formulations. *Eur. J. Pharm. Sci.* 174, 106166. <https://doi.org/10.1016/j.ejps.2022.106166>
- Jamróz, W., Kurek, M., Szafraniec-Szczęsny, J., Czech, A., Gawlak, K., Knapik-Kowalczyk, J., Leszczyński, B., Wróbel, A., Paluch, M., Jachowicz, R., 2020. Speed it up, slow it down...An issue of bicalutamide release from 3D printed tablets. *Eur. J. Pharm. Sci.* 143. <https://doi.org/10.1016/j.ejps.2019.105169>
- Kamble, S., Agrawal, S., Cherumukkil, S., Sharma, V., Jasra, R.V., Munshi, P., 2022. Revisiting zeta potential, the key feature of interfacial phenomena, with applications and recent advancements. *Chemistry Sel.* 7.
- Kanzer, J., Hupfeld, S., Vasskog, T., Tho, I., Hölig, P., Mägerlein, M., Fricker, G., Brandl, M., 2010. In situ formation of nanoparticles upon dispersion of melt extrudate formulations in aqueous medium assessed by asymmetrical flow field-flow fractionation. *J. Pharm. Biomed. Anal.*, 53(3), 359-365. <https://doi.org/10.1016/j.jpba.2010.04.012>
- Karalia, D., Siamidi, A., Karalis, V., Vlachou, M., 2021. 3d- printed oral dosage forms: Mechanical properties, computational approaches and applications. *Pharmaceutics* 13. <https://doi.org/10.3390/pharmaceutics13091401>
- Klar, F., Urbanetz, N.A., 2016. Solubility parameters of hypromellose acetate succinate and plasticization in dry coating procedures. *Drug Dev. Ind. Pharm.* 42, 1621–1635. <https://doi.org/10.3109/03639045.2016.1160106>
- Kumar, A., Pawar, D., Late, D.J., Kanawade, R., 2022. PVA-coated miniaturized flexible fiber optic sensor for acetone detection: a prospective study for non-invasive diabetes diagnosis. *J. Mater. Sci. Mater. Electron.* 33, 2509–2517.



<https://doi.org/10.1007/s10854-021-07458-1>

- Kuźmińska, M., Pereira, B.C., Habashy, R., Peak, M., Isreb, M., Gough, T.D., Isreb, A., Alhnan, M.A., 2021. Solvent-free temperature-facilitated direct extrusion 3D printing for pharmaceuticals. *Int. J. Pharm.* 598, 1–9. <https://doi.org/10.1016/j.ijpharm.2021.120305>
- Lima, A.L., Pires, F.Q., Hilgert, L.A., Sa-Barreto, L.L., Gratieri, T., Gelfuso, G.M., Cunha-Filho, M., 2022. Oscillatory shear rheology as an in-process control tool for 3D printing medicines production by fused deposition modeling. *J. Manuf. Process.* 76, 850–862. <https://doi.org/10.1016/j.jmapro.2022.03.001>
- Madlova, M., Jones, S.A., Zwerschke, I., Ma, Y., Hider, R.C., Forbes, B., 2009. Poly(vinyl alcohol) nanoparticle stability in biological media and uptake in respiratory epithelial cell layers in vitro. *Eur. J. Pharm. Biopharm.* 72, 438–443. <https://doi.org/10.1016/j.ejpb.2009.01.009>
- Mitchell, M.J., Billingsley, M.M., Haley, R.M., Wechsler, M.E., Peppas, N.A., Langer, R., 2021. Engineering precision nanoparticles for drug delivery. *Nat. Rev. Drug Discov.* 20, 101–124. <https://doi.org/10.1038/s41573-020-0090-8>
- Nunes, P.D., Pinto, J.F., Henriques, J., Paiva, A.M., 2022. Insights into the Release Mechanisms of ITZ:HPMCAS Amorphous Solid Dispersions: The Role of Drug-Rich Colloids. *Mol. Pharm.* 19, 51–66. <https://doi.org/10.1021/acs.molpharmaceut.1c00578>
- Pandi, P., Bulusu, R., Kommineni, N., Khan, W., Singh, M., 2020. Amorphous solid dispersions: An update for preparation, characterization, mechanism on bioavailability, stability, regulatory considerations and marketed products. *Int. J. Pharm.* 586, 119560. <https://doi.org/10.1016/j.ijpharm.2020.119560>
- Pereira, G.G., Figueiredo, S., Fernandes, A.I., Pinto, J.F., 2020. Polymer selection for hot-melt extrusion coupled to fused deposition modelling in pharmaceuticals. *Pharmaceutics* 12, 1–63. <https://doi.org/10.3390/pharmaceutics12090795>
- Pietrzak, K., Isreb, A., Alhnan, M.A., 2015. A flexible-dose dispenser for immediate and extended release 3D printed tablets. *Eur. J. Pharm. Biopharm.* 96, 380–387. <https://doi.org/10.1016/j.ejpb.2015.07.027>
- Pires, F.Q., Alves-Silva, I., Pinho, L.A.G., Chaker, J.A., Sa-Barreto, L.L., Gelfuso, G.M., Gratieri, T., Cunha-Filho, M., 2020. Predictive models of FDM 3D printing

- using experimental design based on pharmaceutical requirements for tablet production. *Int. J. Pharm.* 588, 119728. <https://doi.org/10.1016/j.ijpharm.2020.119728>
- Ponsar, H., Wiedey, R., Quodbach, J., 2020. Hot-melt extrusion process fluctuations and their impact on critical quality attributes of filaments and 3d-printed dosage forms. *Pharmaceutics* 12, 1–15. <https://doi.org/10.3390/pharmaceutics12060511>
- Qian, K., Stella, L., Jones, D.S., Andrews, G.P., Du, H., Tian, Y., 2021. Drug-rich phases induced by amorphous solid dispersion: Arbitrary or intentional goal in oral drug delivery? *Pharmaceutics* 13, 1–27. <https://doi.org/10.3390/pharmaceutics13060889>
- Quinten, T., De Beer, T., Remon, J.P., Vervaet, C., 2021. Overview of injection molding as a manufacturing technique for pharmaceutical applications. *Inj. Molding Process. Des. Appl.* 1–42.
- Quintao W.S.C., Ferreira-Nunes R., Gratieri T., Cunha-Filho M., Gelfuso G.M. 2022. Validation of a simple chromatographic method for naringenin quantification in skin permeation experiments. *J Chromatogr B.* 123291. 1201-1202. <https://doi.org/10.1016/j.jchromb.2022.123291>
- Saboo, S., Bapat, P., Moseson, D.E., Kestur, U.S., Taylor, L.S., 2021. Exploring the role of surfactants in enhancing drug release from amorphous solid dispersions at higher drug loadings. *Pharmaceutics* 13, 1–22. <https://doi.org/10.3390/pharmaceutics13050735>
- Schittny, A., Huwyler, J., Puchkov, M., 2020. Mechanisms of increased bioavailability through amorphous solid dispersions: a review. *Drug Deliv.* 27, 110–127. <https://doi.org/10.1080/10717544.2019.1704940>
- Sironi, D., Rosenberg, J., Bauer-Brandl, A., Brandl, M., 2017. Dynamic dissolution-/permeation-testing of nano- and microparticle formulations of fenofibrate. *Eur. J. Pharm. Sci.* 96, 20–27. <https://doi.org/10.1016/j.ejps.2016.09.001>
- Stewart, A.M., Grass, M.E., 2020. Practical Approach to Modeling the Impact of Amorphous Drug Nanoparticles on the Oral Absorption of Poorly Soluble Drugs. *Mol. Pharm.* 17, 180–189. <https://doi.org/10.1021/acs.molpharmaceut.9b00889>
- Thakkar, R., Pillai, A.R., Zhang, J., Zhang, Y., Kulkarni, V., Maniruzzaman, M., 2020. Novel on-demand 3-dimensional (3-d) printed tablets using fill density as an

- effective release-controlling tool. *Polymers* (Basel). 12, 1–21. <https://doi.org/10.3390/POLYM12091872>
- Tho, I., Liepold, B., Rosenberg, J., Maegerlein, M., Brandl, M., Fricker, G., 2010. Formation of nano/micro-dispersions with improved dissolution properties upon dispersion of ritonavir melt extrudate in aqueous media. *Eur. J. Pharm. Sci.* 40(1), 25-32. <https://doi.org/10.1016/j.ejps.2010.02.003>
- Tran, P.H.L., Lee, B.J., Tran, T.T.D., 2021. Recent studies on the processes and formulation impacts in the development of solid dispersions by hot-melt extrusion. *Eur. J. Pharm. Biopharm.* 164, 13–19. <https://doi.org/10.1016/j.ejpb.2021.04.009>
- Ullmann, C., Babick, F., Stintz, M., 2019. Microfiltration of submicron-sized and nano-sized suspensions for particle size determination by dynamic light scattering. *Nanomaterials* 9. <https://doi.org/10.3390/nano9060829>
- van Krevelen, D.W., te Nijenhuis, K., 2009. *Properties of polymers: Their correlation with chemical structure; Their numerical estimation and prediction from additive group contributions.*, 4th Editio. ed. Elsevier Science.
- Wilson, V.R., Mugheirbi, N.A., Mosquera-Giraldo, L.I., Deac, A., Moseson, D.E., Smith, D.T., Novo, D.C., Borca, C.H., Slipchenko, L. V., Edgar, K.J., Taylor, L.S., 2021. Interaction of Polymers with Enzalutamide Nanodroplets - Impact on Droplet Properties and Induction Times. *Mol. Pharm.* 18, 836–849. <https://doi.org/10.1021/acs.molpharmaceut.0c00833>
- Yang, R., Mann, A.K.P., Van Duong, T., Ormes, J.D., Okoh, G.A., Hermans, A., Taylor, L.S., 2021. Drug Release and Nanodroplet Formation from Amorphous Solid Dispersions: Insight into the Roles of Drug Physicochemical Properties and Polymer Selection. *Mol. Pharm.* 18, 2066–2081. <https://doi.org/10.1021/acs.molpharmaceut.1c00055>
- Yang, Y., Wang, H., Xu, X., Yang, G., 2021. Strategies and mechanisms to improve the printability of pharmaceutical polymers Eudragit® EPO and Soluplus®. *Int. J. Pharm.* 599. <https://doi.org/10.1016/j.ijpharm.2021.120410>
- Zheng, T., Bott, S., Huo, Q., 2016. Techniques for Accurate Sizing of Gold Nanoparticles Using Dynamic Light Scattering with Particular Application to Chemical and Biological Sensing Based on Aggregate Formation. *ACS Appl. Mater. Interfaces* 8, 21585–21594. <https://doi.org/10.1021/acsami.6b06903>

**FIGURES CAPTIONS**

Journal Pre-proof

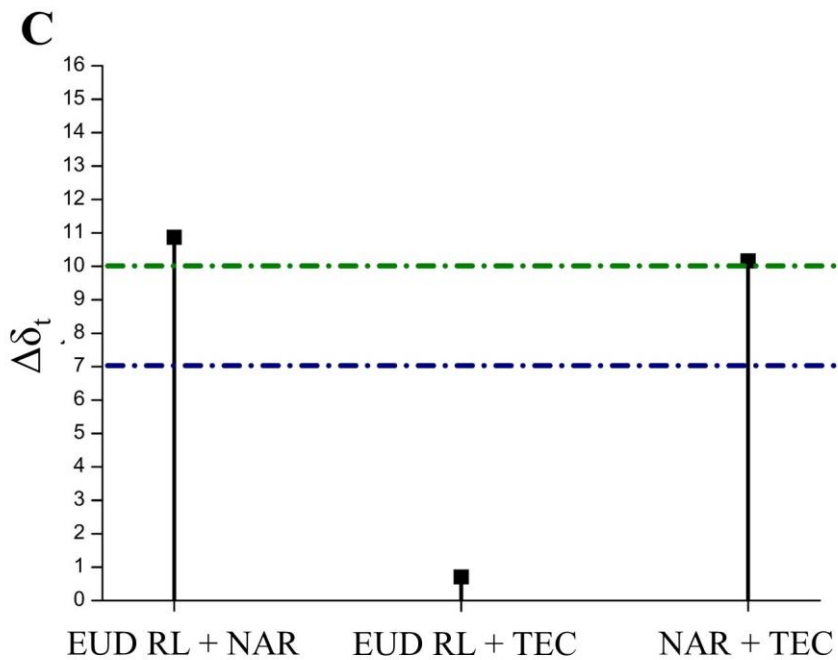
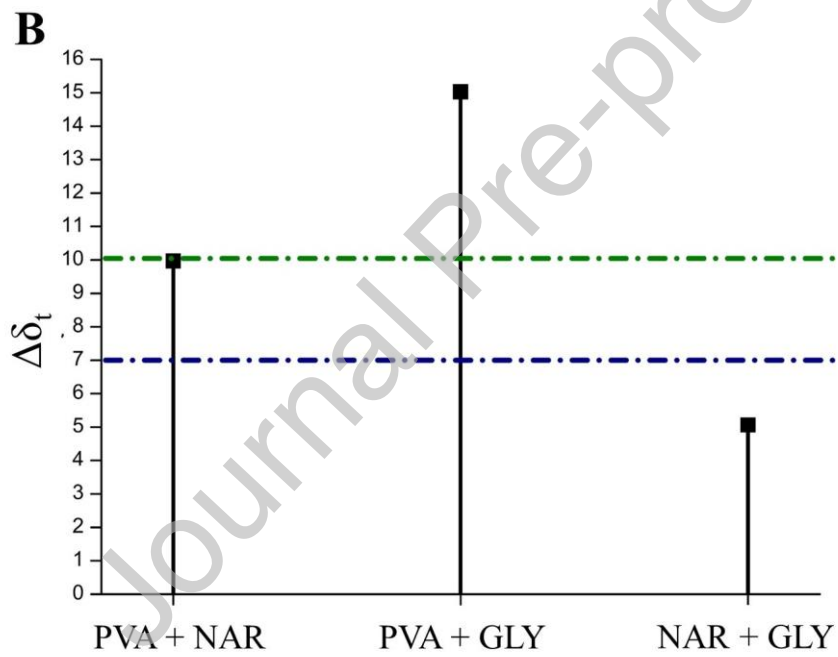
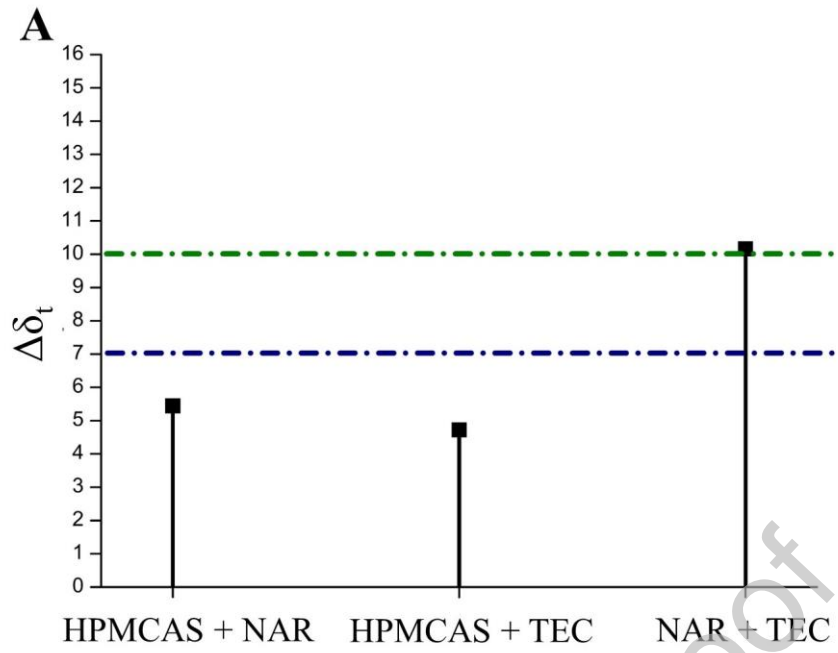


**Fig. 1.** Variation of the total Hansen solubility parameter ( $\Delta\delta_t$ ) of each combination of materials related to the polymer-based formulations of hydroxypropylmethylcellulose acetate succinate (HPMCAS) and the plasticizer triethyl citrate (TEC) (A), Polyvinyl alcohol (PVA) and the plasticizer Glycerin (GLY) (B), and Eudragit RL PO<sup>®</sup> (EUD RL) and the plasticizer TEC (C). The blue line represents the limit for high interactions (up to 7.0 MPa<sup>1/2</sup>), and the green line is the limit for low interactions (up to 10.0 MPa<sup>1/2</sup>).

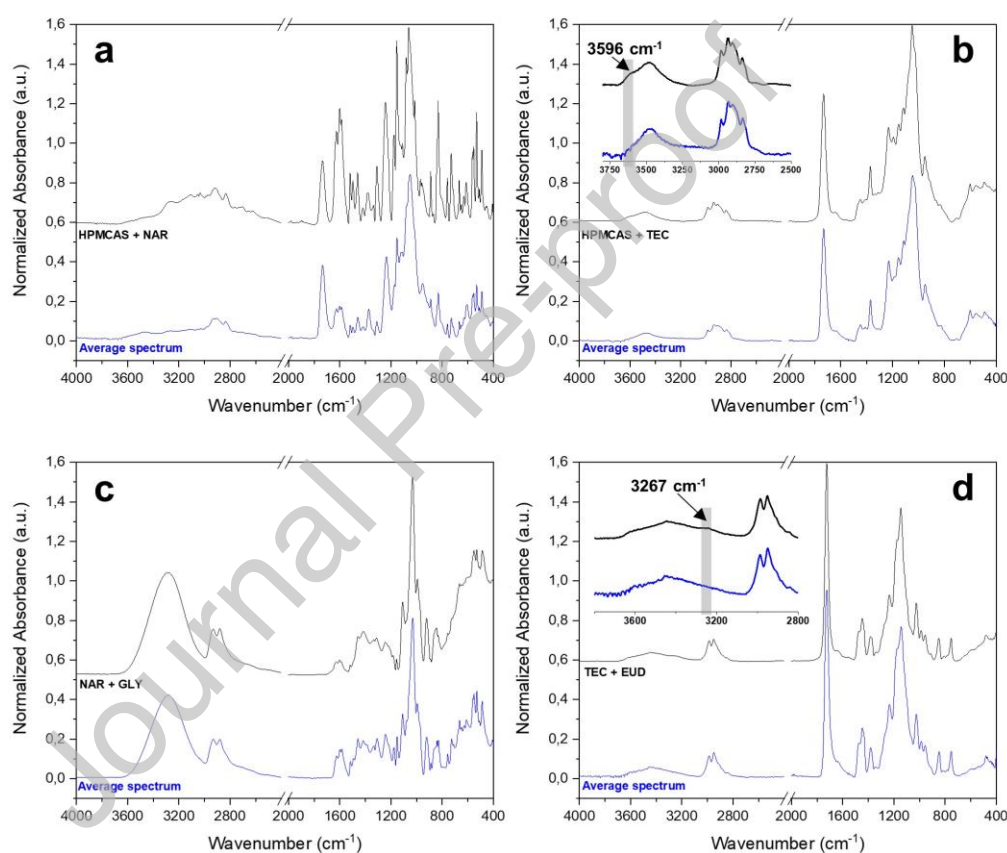


**Fig. 2.** FTIR spectra of the selected samples: a) hydroxypropylmethylcellulose acetate succinate (HPMCAS) and Naringenin (NAR); b) HPMCAS and triethyl citrate (TEC); c) Glycerin (GLY) and NAR; and d) Eudragit RL PO<sup>®</sup> (EUD RL) and TEC. The calculated average spectrum was obtained by the combination of the pure material spectra data considering the proportion of each component in the mixture.

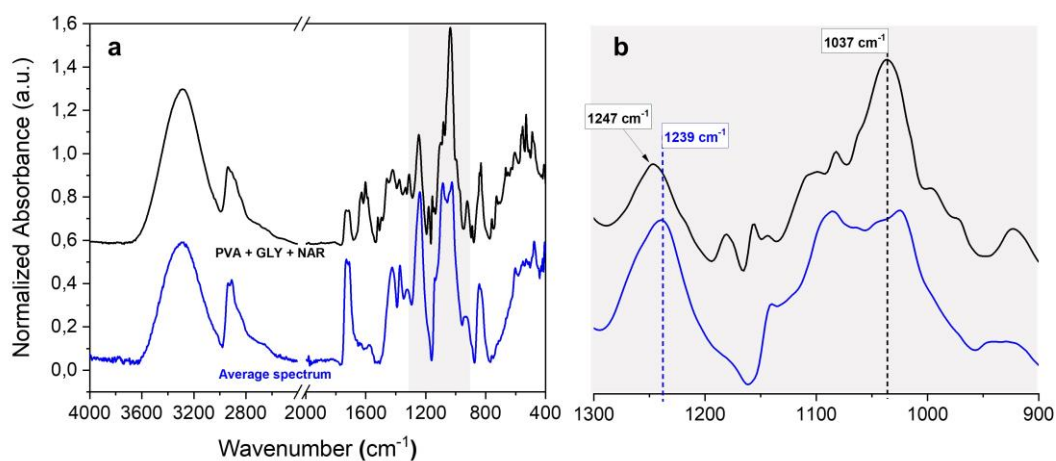


**Fig. 3.** a) FTIR spectra of the physical mixture and calculated average spectrum for PVA/GLY/NAR ternary system; b) Zoom of the highlighted gray shaded rectangle region, from 1,300 to 900  $\text{cm}^{-1}$ . PVA - Polyvinyl alcohol, GLY – Glycerin and NAR – Naringenin.

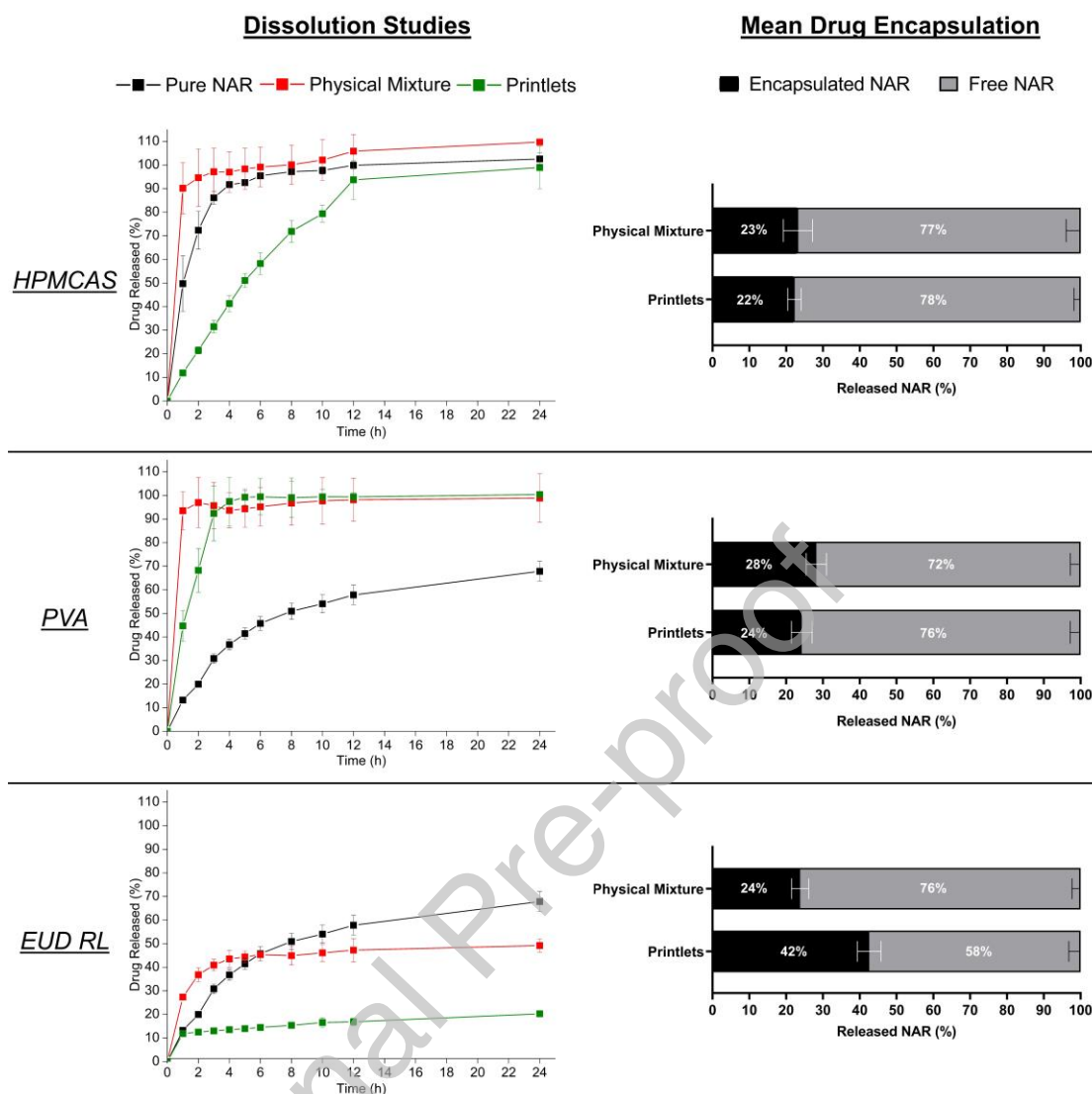


**Fig. 4.** Dissolution profile and mean encapsulation of the released Naringenin (NAR) through 24 h experiment for the printlets produced with the polymers hydroxypropylmethylcellulose acetate succinate (HPMCAS), Polyvinyl alcohol (PVA), and Eudragit RL PO<sup>®</sup> (EUD RL) and the control samples, pure NAR, and physical mixture. Since the drug encapsulation values were stable, the mean drug encapsulation considers the values obtained during the experiment.



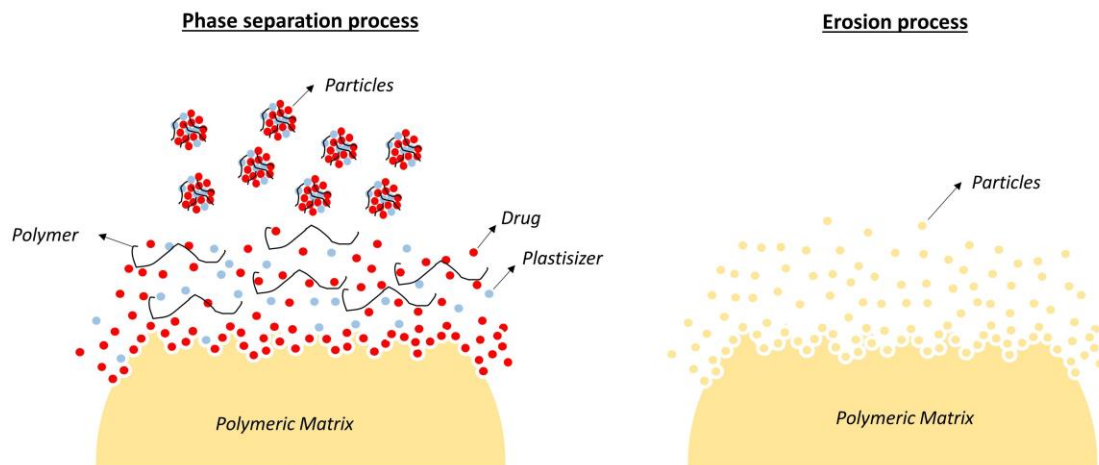
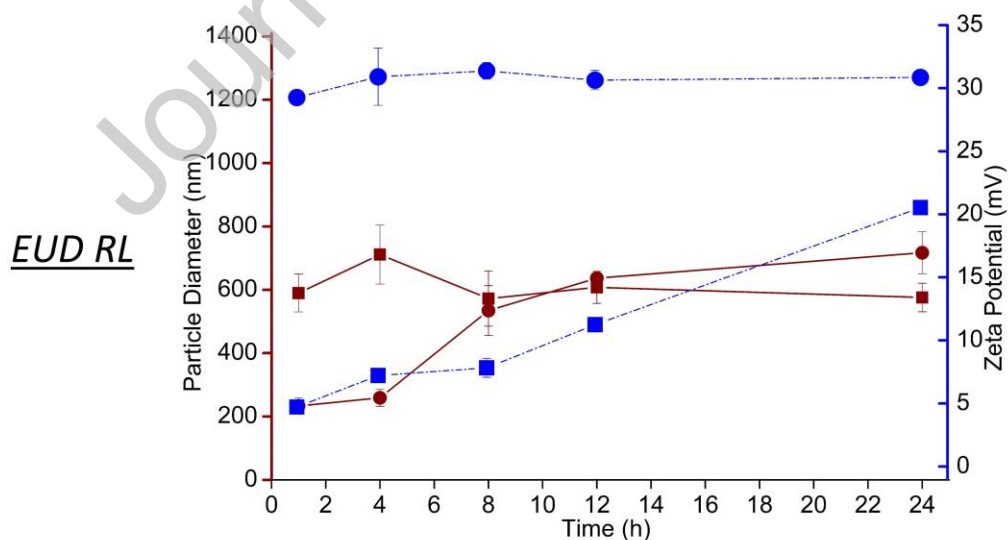
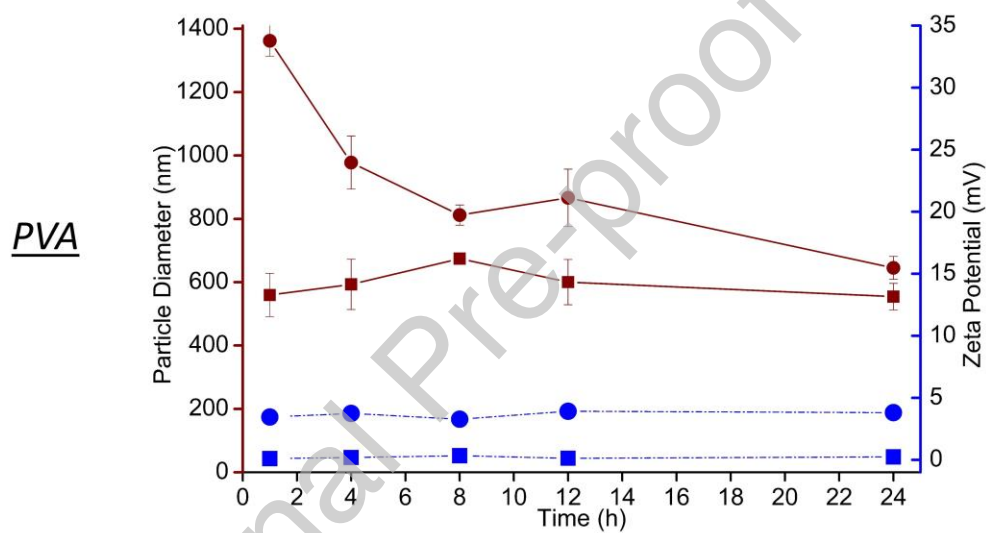
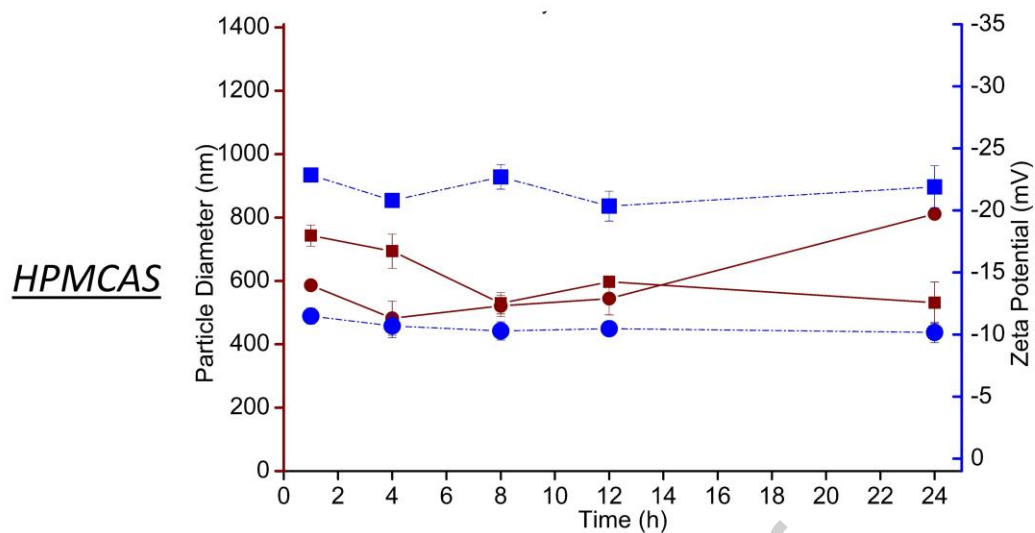


**Fig. 5.** Graphical representation of two theoretical pathways of particle formation, phase separation, and erosion.



—■— Particle Diameter - Physical Mixture   
 —●— Particle Diameter - Printlets  
- -■- - Zeta Potential - Physical Mixture   
 - -●- - Zeta Potential - Printlets

**Fig. 6.** Particle diameter and zeta potential of the particles arose spontaneously from the dissolution of the physical mixtures and the printlets over 24h, produced with the polymers hydroxypropylmethylcellulose acetate succinate (HPMCAS), Polyvinyl alcohol (PVA), and Eudragit RL PO<sup>®</sup> (EUD RL).

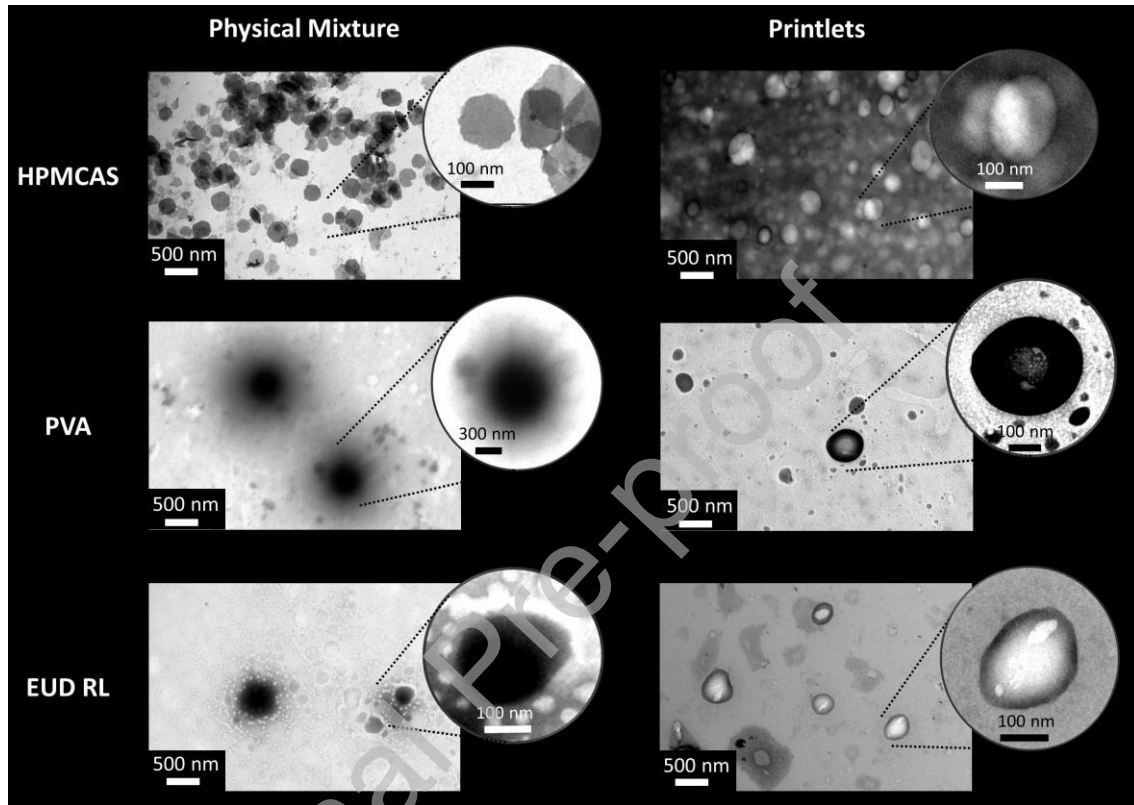
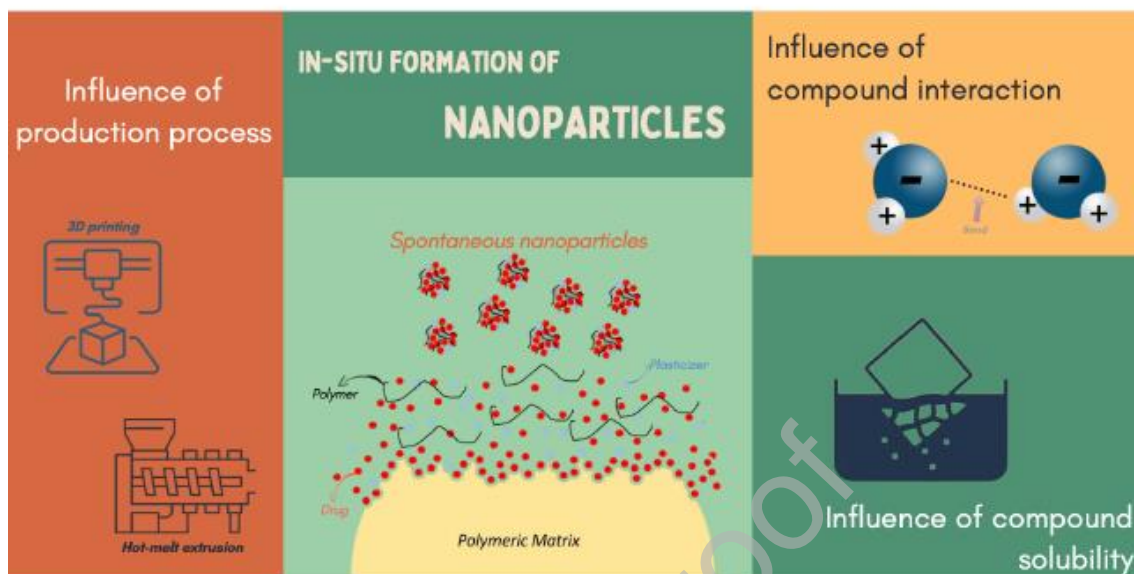


**Fig. 7.** TEM images of the particles arose spontaneously from the dissolution of the physical mixtures and the printlets after 24h produced with the polymers hydroxypropylmethylcellulose acetate succinate (HPMCAS), Polyvinyl alcohol (PVA), and Eudragit RL PO<sup>®</sup> (EUD RL).



Graphical abstract

### CRedit authorship contribution statement

**Felipe Q. Pires:** Investigation, Methodology, Writing – original draft. **Idejan P. Gross:** Investigation, Writing – review & editing. **Livia L. Sa-Barreto:** Resources, Project administration. **Tais Gratieri:** Conceptualization, Writing – review & editing. **Guilherme M. Gelfuso:** Conceptualization, Writing – review & editing. **Sonia N. Bao:** Methodology, Writing – review & editing. **Marcilio Cunha-Filho:** Conceptualization, Supervision, Writing – review & editing.

## TABLES

**Table 1.** Formulations composition (% , m/m) with the amount of plasticizer and model drug. HPMCAS - hydroxypropylmethylcellulose acetate succinate, PVA - Polyvinyl alcohol, EUD RL - Eudragit RL PO<sup>®</sup>, TEC - Triethyl citrate, GLY – Glycerin and NAR – Naringenin.







Formulation	Plasticizer		Model Drug	
	GLY	TEC	NAR	
With NAR	HPMCAS	-	20%	5%
	PVA	20%	-	5%
	EUD RL	-	13%	5%
Without NAR	HPMCAS	-	20%	-
	PVA	20%	-	-
	EUD RL	-	13%	-

**Table 2.** Hansen solubility parameters.  $\delta_d$  – Dispersion parameter;  $\delta_p$  – Polar parameter;  $\delta_h$  – Hydrogen bonds parameter;  $\delta_t$  – Total Hansen solubility parameter. HPMCAS - hydroxypropylmethylcellulose acetate succinate, PVA - Polyvinyl alcohol, EUD RL - Eudragit RL PO<sup>®</sup>, TEC - triethyl citrate and GLY - Glycerin.






Material	Hansen solubility parameters (MPa <sup>1/2</sup> )			
	$\delta_d$	$\delta_p$	$\delta_h$	$\delta_t$
NAR	22.71	9.68	18.98	31.14

<i>HPMCAS</i>	20.50	5.10	14.60	25.70
<i>PVA</i>	11.20	12.40	13.00	21.17
<i>EUD RL</i>	16.92	1.02	11.11	20.27
<i>TEC</i>	16.50	4.90	12.00	20.98
<i>GLY</i>	17.40	12.10	29.30	36.20

**Table 3.** Filaments manufacturing specifications and characterization data of all formulations with and without naringenin (NAR). HPMCAS - hydroxypropylmethylcellulose acetate succinate, PVA - Polyvinyl alcohol, EUD RL - Eudragit RL PO<sup>®</sup>,  $T_{\text{extrusion}}$  – Extrusion temperature and  $V_{\text{rotation}}$  - Velocity of the screws rotation.

Formulation	$T_{\text{extrusion}}$	$V_{\text{rotation}}$	Mean	Fracture	Aspect	
	n (°C)	n (RPM)	Diameter (mm)	Force (N)		
<b>With NAR</b>	HPMCA S	140 4	30 3	1.67±0.0 4	28.77±1.1 3	
	PVA	150 4	30 9	1.70±0.0 4	28.79±2.5 9	
	EUD RL	140 6	40 8	1.46±0.0 6	24.34±1.3 8	
<b>Without NAR</b>	HPMCA S	140 6	30 2	1.62±0.0 6	30.59±1.5 2	
	PVA	150 1	30 6	1.59±0.1 1	28.19±1.1 6	
	EUD RL	140 7	40 2	1.59±0.0 7	22.29±1.8 2	

**Table 4.** Printlets manufacturing specifications and characterization data of all formulations with and without naringenin (NAR). HPMCAS - hydroxypropylmethylcellulose acetate succinate, PVA - Polyvinyl alcohol, EUD RL - Eudragit RL PO<sup>®</sup> and T<sub>printing</sub> – printing temperature.

Formulation	T <sub>printing</sub> (°C)	Volume (cm <sup>3</sup> )	Weight (g)	Drug content (%)	Aspect	
<i>HPMCAS</i>	180	0.579±0.005	0.408±0.010	94.9±0.8		
<b>With NAR</b>	<i>PVA</i>	180	0.605±0.005	0.637±0.027	102.5±0.8	
	<i>EUD RL</i>	190	0.551±0.007	0.523±0.022	93.2±0.9	
	<i>HPMCAS</i>	180	0.568±0.004	0.463±0.014	-	
<b>Without NAR</b>	<i>PVA</i>	180	0.563±0.009	0.525±0.010	-	
	<i>EUD RL</i>	190	0.549±0.007	0.471±0.013	-	